

Nanoscale

Accepted Manuscript



This is an *Accepted Manuscript*, which has been through the Royal Society of Chemistry peer review process and has been accepted for publication.

Accepted Manuscripts are published online shortly after acceptance, before technical editing, formatting and proof reading. Using this free service, authors can make their results available to the community, in citable form, before we publish the edited article. We will replace this *Accepted Manuscript* with the edited and formatted *Advance Article* as soon as it is available.

You can find more information about *Accepted Manuscripts* in the [Information for Authors](#).

Please note that technical editing may introduce minor changes to the text and/or graphics, which may alter content. The journal's standard [Terms & Conditions](#) and the [Ethical guidelines](#) still apply. In no event shall the Royal Society of Chemistry be held responsible for any errors or omissions in this *Accepted Manuscript* or any consequences arising from the use of any information it contains.

Cite this: DOI: 10.1039/c0xx00000x

www.rsc.org/xxxxxx

ARTICLE TYPE

Boron dipyrromethene (BODIPY) Functionalized Carbon Nano-Onions for High Resolution Cellular Imaging

Juergen Bartelmess,^a Elisa De Luca,^b Angelo Signorelli,^a Michele Baldrighi,^a Michele Becce,^a Rosaria Brescia,^c Valentina Nardone,^{d,e} Emilio Parisini,^d Luis Echegoyen,^f Pier Paolo Pompa^b and Silvia Giordani^{*a}

Received (in XXX, XXX) Xth XXXXXXXXX 20XX, Accepted Xth XXXXXXXXX 20XX

DOI: 10.1039/b000000x

Carbon nano-onions (CNOs) are an exciting class of carbon nanomaterials, which have recently demonstrated facile cell-penetration capabilities. In the present work, highly fluorescent boron dipyrromethene (BODIPY) dyes were covalently attached to the surface of CNOs. The introduction of this new carbon nanomaterial-based imaging platform, made of CNOs and BODIPY fluorophores, allows for the exploration of synergetic effects between the two building blocks and for the elucidation of its performance in biological applications. The high fluorescence intensity exhibited by the functionalized CNOs translates into an excellent *in vitro* probe for the high resolution imaging of MCF-7 human breast cancer cells. It was also found that the CNOs, internalized by the cells by endocytosis, are localized in the lysosomes and did not show any cytotoxic effects. The presented results highlight CNOs as excellent platforms for biological and biomedical studies due to their low toxicity, efficient cellular uptake and low fluorescence quenching of attached probes.

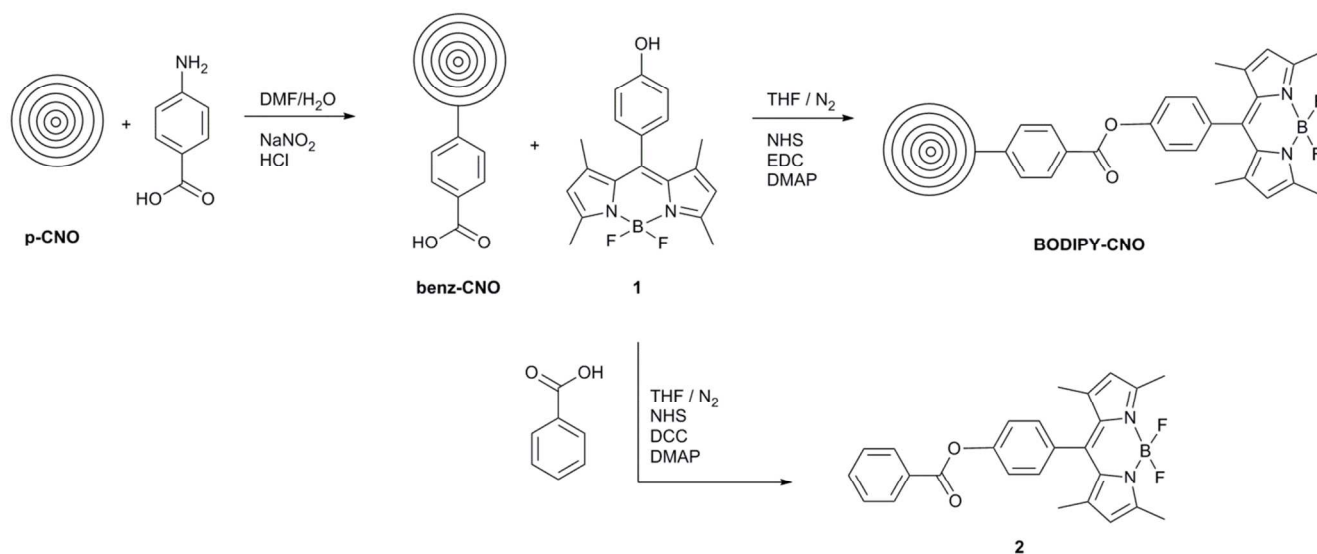
Introduction

In the flourishing research field of nanomedicine, the outstanding results provided by carbon nanomaterials are continuously stimulating their improvement in different areas, such as regenerative medicine, drug delivery and bioimaging.^{1,2,3} For these purposes, fullerenes,^{4,5,6} carbon nanotubes,^{7,8} nanodiamonds^{9,10} and graphene based nanostructures^{11,12} were recently investigated, providing excellent results and showing in some cases the possibility of combining multiple features on a single nano-platform.¹ In the search for the best (*i.e.* the most effective and the least toxic) nano-vector, carbon nano-onions (CNOs)¹³ have played, until now, only a minor role. Their possible application in nanomedicine has not been fully explored, despite extensive investigations in other fields of research,¹⁴ such as tribology,^{15,16} sensing,^{17,18} catalysis,¹⁹ and their use in supercapacitors.^{20,21,22} Their application in the context of biomedicine is limited to very few examples,^{17,23} in which few-layer (≈ 5 nm average diameter) CNOs have demonstrated very promising properties in cell penetration, along with low cytotoxicity and low inflammatory potential.²³ Furthermore, following synthetic strategies developed for other carbon nanomaterials,²⁴ pristine CNOs (p-CNOs) can be decorated with a large variety of functional groups.^{14,25} A common reaction for covalent CNO functionalization is the so-called *Tour* reaction,²⁶ which allows for the introduction of a large variety of functional groups,²⁵ like for example benzoic acid.

The fluorescent tag used in this study is a boron dipyrromethene (BODIPY) derivative. BODIPY dyes show excellent optical

properties like high molar extinction coefficients as well as high fluorescence quantum yields in combination with good stability.^{27,28} They are therefore widely used as imaging agents in biology.^{29,30,31} In addition, the application of BODIPY dyes in systems for solar energy conversion,^{32,33,34,35} light-driven hydrogen generation,³⁶ and for photodynamic therapy of cancer^{37,38} has been studied. Electrogenerated chemiluminescence³⁹ and fluorescence sensing⁴⁰ have also been described for a variety of BODIPY derivatives. The synthetic versatility of the BODIPY chromophore is well documented and allows for a wide range of structural modifications, altering the dyes' electronic, optical and chemical properties.^{27,28,41,42}

In earlier studies, the further functionalization of carboxylic or benzoic acid decorated CNOs was accomplished by condensation reactions with primary amines leading to amides.^{14,17,23} In the present study, we report for the first time the esterification of benzoic acid functionalized small diameter (≈ 5 nm) CNOs with *meso*-phenol substituted boron dipyrromethene (BODIPY) fluorophore **1**.⁴³ To the best of our knowledge, it is also the first report of the use of a *meso*-phenol substituted BODIPY as a substrate for a Steglich-type esterification reaction with benzoic acid derivatives. All carbon nanomaterials were characterized by means of Raman and attenuated total reflectance Fourier transform infrared spectroscopy (ATR-FTIR), thermogravimetric analysis (TGA), UV-vis absorption and fluorescence spectroscopy, dynamic light scattering (DLS), Z-potential, low and high resolution transmission electron microscopy (LRTEM and HRTEM), electron energy loss spectroscopy (EELS) and atomic force microscopy (AFM). The cellular uptake mechanisms



Scheme 1 Synthetic procedure for the synthesis of BODIPY functionalized CNOs (**BODIPY-CNO**) and the corresponding benzoic acid ester (**2**).

of the CNO nanomaterials by MCF-7 (Michigan Cancer
 5 Foundation-7) breast cancer cells and the intracellular localization
 of the fluorescent CNOs were elucidated. In combination with
 toxicological studies, this work highlights the excellent properties
 of CNO based nanomaterials for biological imaging and
 encourages future studies with CNOs as molecular shuttles for
 10 targeted drug delivery.

were synthesized by an ester condensation reaction (Scheme 1).
 The raw CNO material (**p-CNO**) was prepared by the annealing
 of nanodiamonds particles with a diameter of approx. 5 nm,
 25 following reported procedures.^{44,45,46} Benzoic acid functionalities
 were introduced by reacting **p-CNOs** with 4-aminobenzoic acid
 and sodium nitrite in an acidified DMF/water mixture, an
 adaptation of the *Tour* reaction.^{23,25,26} Subsequently, **benz-CNOs**
 were reacted with *N*-hydroxysuccinimide (NHS) and the *meso*-
 30 phenol substituted BODIPY **1**.⁴³ The esterification reaction was
 carried out in the presence of 1-ethyl-3-(3-dimethylaminopropyl)
 carbodiimide (EDC) (or *N,N'*-dicyclohexylcarbodiimide – DCC,
 as indicated in Scheme 1) and 4-(dimethylamino)pyridine
 (DMAP) in dry THF. The **BODIPY-CNO** nanomaterial was
 35 purified by subsequent centrifugation and several re-dispersion
 steps in THF, while **2** was purified by column chromatography.

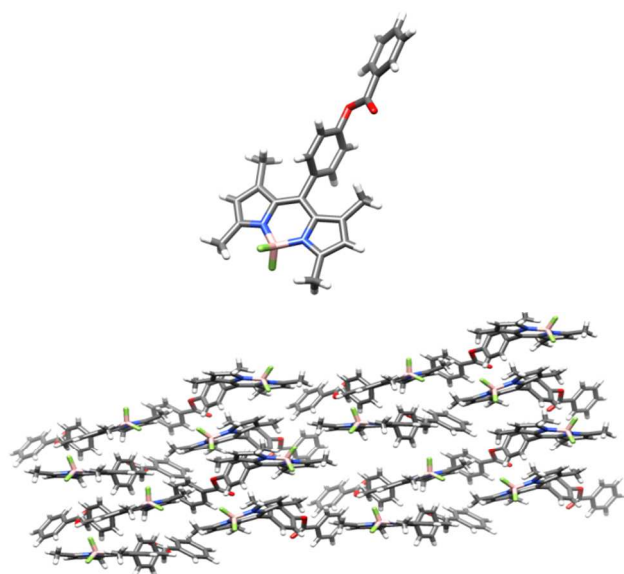


Fig. 1 Crystal structure of **2**. Structure of a single BODIPY-ester
 molecule (top) and the remarkable high-symmetry crystal cell, containing
 15 16 symmetry-generated molecules (bottom). Color code: pink: boron;
 grey: carbon; green: fluorine; light gray: hydrogen; blue: nitrogen; red:
 oxygen.

Results and discussion

Synthetic Aspects

20 BODIPY functionalized CNOs (**BODIPY-CNOs**) and the related
 benzoic acid-BODIPY ester (**2**), used as reference compound,

Reference compound 2

The reference compound **2** was synthesized to study the
 40 spectroscopic properties of this new BODIPY fluorophore
 without being influenced by the presence of the CNO
 nanomaterial. In general, a close connection between carbon
 nanomaterials and chromophores makes it difficult to investigate
 the properties of the bound chromophore in great detail. Usually,
 45 a broadening and weakening of the fluorescence signal is
 observed, mainly due to the size and strong intrinsic absorption of
 the carbon nanostructures and to possible electronic
 interactions.^{23,47,48}

X-ray quality crystals of **2** were obtained as orange rhombic
 50 plates by re-crystallization from dichloromethane / methanol (1:3
 v/v) at -20°C. The diffraction derived structure of **2** is presented
 in Figure 1;[‡] additional details, tables and a numbering Scheme
 for the molecule are provided in the ESI. **2** crystallizes in the
 orthorhombic crystal system, space group *Fdd2*. The boron atom
 55 is coordinated in a tetrahedral geometry by two nitrogen and two
 fluorine atoms. The BODIPY core is near-planar, and the
 dihedral angle between the two pyrrole rings is 9.58°. The

planarity of the indacene core, which forms an extended conjugated system, is an essential requirement for the optical properties of this class of compounds. The *meso*-phenyl group is nearly orthogonal to the indacene 12-member cycle, with the two moieties forming an angle of 79.9(6)°. This conformation limits the possible resonance between the indacene core and the phenyl ring, as also demonstrated by the rather long [1.505(7) Å] chemical bond between them, a distance consistent with a single bond character. The orientation of the phenyl group allows the formation of a stabilizing CH- π hydrogen bond [2.91 Å] between one of the methyl groups on the indacene core and the centroid of the aromatic ring. The benzoic group orients at an angle of 38.82° relative to the BODIPY core plane and at an angle of 58.96° with respect to the plane of the phenyl group. This last value shows a lack of extensive π -coupling between the two phenyl rings, although partial delocalization involving the carboxylate group is still possible. Indeed, the rather short carboxylic C-O distance [1.406(6) Å] indicates a partial double bond character. The crystal packing of **2** appears to be mainly stabilized by a number of hydrogen bonds between aromatic hydrogen atoms and the fluorine and oxygen atoms in the molecule. Neither the indacene core nor the phenyl rings show any evidence of stabilizing π - π stacking interactions.

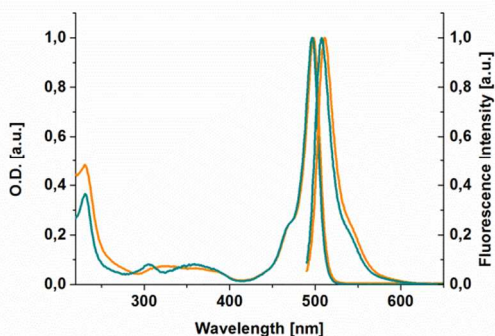


Fig. 2 Normalized absorption (left axis) and fluorescence (right axis) spectra of **1** (green) and **2** (orange) in acetonitrile. Excitation at 485 nm.

The spectroscopic data for compound **2** in various solvents are summarized in Table 1. Briefly, the absorption spectra of **2** in toluene shows an absorption maximum at 504 nm with a molar extinction coefficient of $91.8 \times 10^3 \text{ M}^{-1} \text{ cm}^{-1}$. A minor solvent dependency is observed. In acetonitrile the absorption maximum undergoes a hypsochromic shift of 6 nm to 498 nm. The emission maximum of **2** in toluene is located at 517 nm with a fluorescence quantum yield of 0.60, while the emission maximum in acetonitrile is at 511 nm with a fluorescence quantum yield of 0.51. For comparison, **1** in toluene has an absorption maximum at 503 nm, an emission maximum at 515 nm, and a slightly higher fluorescence quantum yield (0.64).⁴⁹ When comparing the absorption spectra of **1** and **2** in acetonitrile, an increased absorption is observed for the latter in the UV-region, with a maximum at 231 nm (Figure 2). This can be attributed to the absorption of the phenyl group of the benzoic ester moiety. ATR FTIR spectroscopy reveals the presence of a carbonyl stretching band at 1738 cm^{-1} and no -OH functionality (Figure S2), corroborating the successful esterification of **1** with benzoic acid, leading to **2**.

Table 1 Photophysical data of **2** in toluene, dichloromethane (DCM), DMSO and acetonitrile.

Solvent	λ_{Abs} [nm]	ϵ [$\times 10^3 \text{ M}^{-1} \text{ cm}^{-1}$]	λ_{Em} [nm]	Stokes Shift [nm]	Φ_{F}
toluene	504	91.8	517	13	0.60
DCM	502	103.6	516	14	0.57
DMSO	502	86.4	516	14	0.67
acetonitrile	498	87.5	511	13	0.51

Characterization of the CNOs

BODIPY-CNOs were characterized by a wide variety of analytical, spectroscopic and microscopic techniques. Full characterization of the efficiency of nanodiamond conversion and the purity of the **p-CNOs** was obtained using a combination of TGA, HRTEM (with EELS), Raman and FTIR spectroscopy. Similar techniques were used for the characterization of **benz-CNOs**, verifying a successful covalent CNO functionalization with benzoic acid by the Tour reaction.

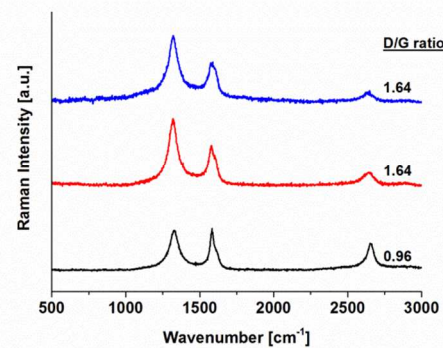


Fig. 3 Raman spectra of **p-CNOs** (black), **benz-CNOs** (red) and **BODIPY-CNOs** (blue). Raman spectra normalized for the G-band at 1580 cm^{-1} , the ratios of the D-band to the G-band intensities are indicated.

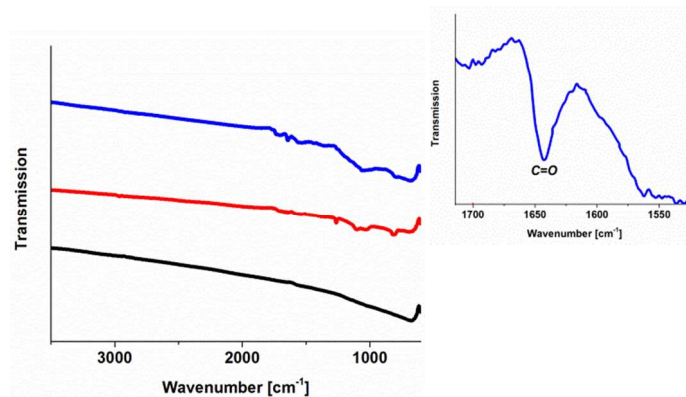


Fig. 4 ATR FTIR spectra of **p-CNOs** (black), **benz-CNOs** (red) and **BODIPY-CNOs** (blue). Inset: magnification of the carbonyl region in the IR-spectrum of **BODIPY-CNOs**.

Raman spectroscopy indicated a successful covalent functionalization of the **p-CNO** starting material, reflected as an increase of the D-band at 1320 cm^{-1} , compared to the G-band at 1580 cm^{-1} (Figure 3). The D/G ratio increases from 0.96 for the **p-CNOs** to 1.64 for the **benz-CNOs** and for **BODIPY-CNOs**, demonstrating the covalent functionalization of the **p-CNOs**. FTIR spectroscopy proved the nature of the functional groups

introduced basing on their characteristic stretching vibrations. While **p-CNOs** showed no significant IR bands, **benz-CNOs** displayed some distinct IR bands in the region between 620 and 1800 cm^{-1} , which changed significantly upon esterification with **1** (Figure 4). The most distinctive feature is a carbonyl band at around 1640 cm^{-1} (Figure 4, Inset).

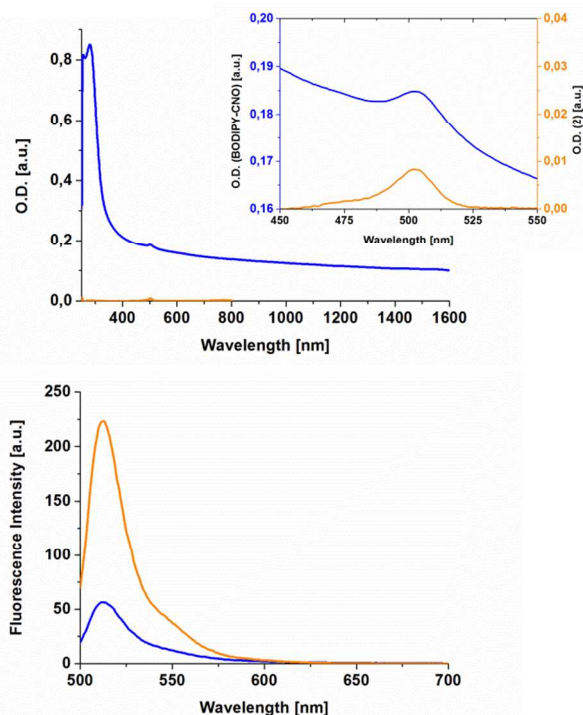


Fig. 5 Absorption spectra (top) and corresponding fluorescence spectra (bottom) of **BODIPY-CNOs** (blue) and **2** (orange) in DMSO. Inset: Magnification of the BODIPY centered absorption features in **BODIPY-CNOs** and **2** with comparable BODIPY absorption intensity at the excitation wavelength of 490 nm.

Thermogravimetric analysis confirm the successful functionalization of the CNOs (Figure S3). **p-CNOs** decompose at around 570 $^{\circ}\text{C}$, without any weight loss at lower temperatures. **Benz-CNOs** revealed significant weight loss starting at around 150 $^{\circ}\text{C}$ and decomposed completely at around 570 $^{\circ}\text{C}$ as well. In the low temperature domain, the weight loss of **BODIPY-CNOs** was significantly larger due to an increased organic functionalization with BODIPY fluorophores. The degree of functionalization of the CNO nanomaterial was estimated from the weight losses, as described in the literature,⁵⁰ assuming that one CNO consists of 6 carbon shells. The TGA of **benz-CNOs** and **BODIPY-CNOs** performed in air show a weight loss at 400 $^{\circ}\text{C}$ of about 10% and additional 18% respectively. We estimated about 55 benzoic acid functionalities per onion for **benz-CNOs** and approx. 37 BODIPY molecules per CNO for **BODIPY-CNOs**.

UV-vis-NIR absorption spectroscopy of **BODIPY-CNOs** revealed the typical absorption features of CNOs as a broad plasmonic absorption over the whole spectral range (Figure 5) and a distinct absorption band, with a maximum at 502 nm in dimethyl sulfoxide (DMSO), which can be attributed to BODIPY. Upon photoexcitation, fluorescence emission with a maximum at 512 nm was observed. Comparison of the maximum fluorescence intensities of a **BODIPY-CNO** dispersion with that of a solution

of **2** in DMSO allowed for an estimation of the **BODIPY-CNOs** fluorescence quantum yield with a value of about 0.17 (*i.e.* 25% of the fluorescence quantum yield of **2**). The BODIPY centered absorption at the excitation wavelength of 490 nm was similar for both samples. All spectroscopic results support the successful covalent functionalization of CNOs with the bright fluorescent BODIPY dye. Notably, while many other dye molecules covalently linked to different carbon nanostructures exhibit a strong fluorescence quenching, which limits their use in imaging applications,^{51,52,53} **BODIPY-CNOs** largely overcome this problem. The attachment of BODIPY to the CNOs leads in fact just to a small reduction of the fluorescence emission. This fluorescence quenching observed for **BODIPY-CNOs** can be ascribed to the high absorption of the bulk CNO material and not to electron / energy transfer events, which usually results in very pronounced fluorescence quenching. These conclusions are consistent with our recent report using NIR fluorescent BF_2 -chelates of azadipyromethene dyes in combination with CNOs,⁵⁴ and very promising for the design and application of fluorescent labels based on CNOs for biological imaging.

DLS and Z-potential measurements were performed in order to characterize the nanoparticles' behavior under physiological conditions (Table S2). DLS measurements were performed in phosphate buffered saline (PBS) at pH 7.4 to mimic the conditions used in biological experiments. Initially, **benz-CNOs** and **BODIPY-CNOs** were dissolved in DMSO at a concentration of 1.0 mg/mL and then diluted with PBS to a final concentration of 10 $\mu\text{g}/\text{mL}$. Z-potential measurements were conducted instead in a low ionic strength medium (phosphate buffer 0.01 M pH 7.4), at a 20 $\mu\text{g}/\text{mL}$ CNO concentration and without prior dispersion in DMSO, in order not to alter the characteristics of their surface. Under these conditions, **BODIPY-CNO** agglomerates show a bimodal dimensional distribution, featuring averages of 110 ± 16 nm (43%) and 426 ± 93 nm (57%), which display a Z-potential of -23 mV. As expected, this value is less negative than the one found for **benz-CNOs**, -39.7 mV.

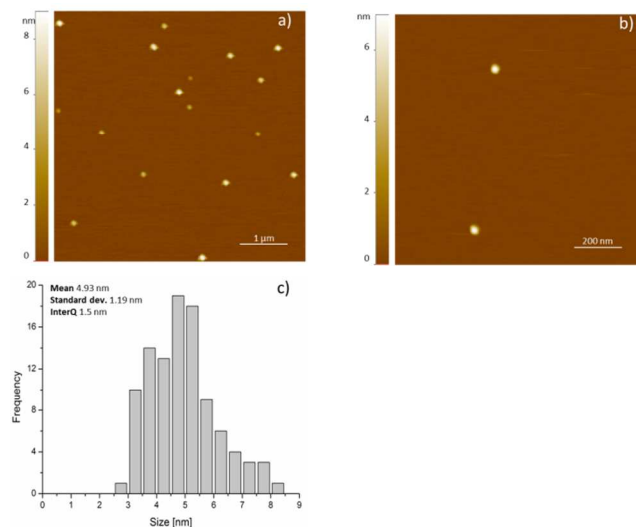


Fig. 6 AFM of **BODIPY-CNOs**. a) and b) topographs of CNOs at different magnification c) size distribution analysis.

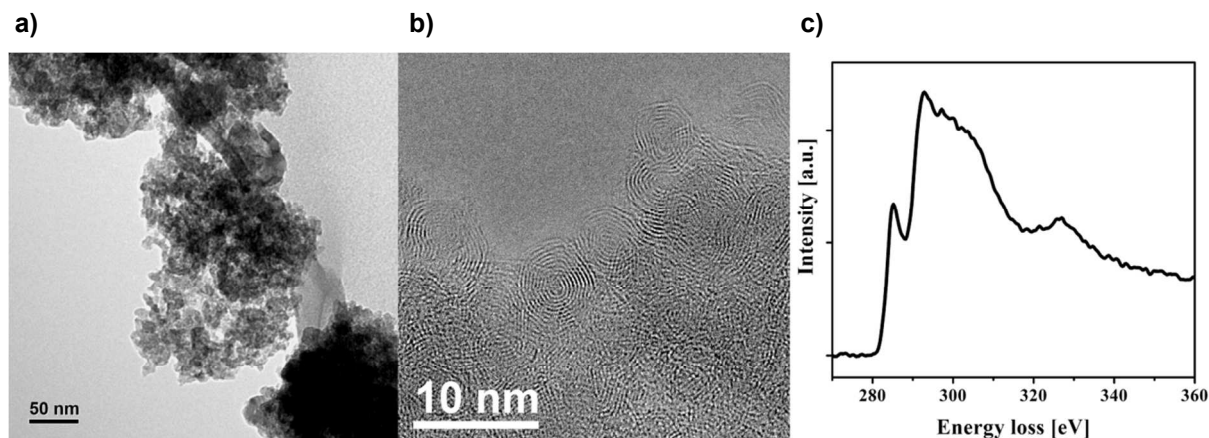


Fig. 7 a) Overview BF-TEM image of a **BODIPY-CNO** aggregate. b) HR-TEM image of peripheral **BODIPY-CNOs** in an aggregate partly suspended on a hole. The measured intershell spacing is 3.4 Å. c) Single-scattering EEL spectrum at the carbon K-edge collected from a **BODIPY-CNO** aggregate suspended on vacuum, showing the typical near-edge fine structure reported for CNOs.⁵⁵

AFM analyses were performed in order to estimate the size of the nano-onions. Figure 6 illustrates two typical topographic images of individual **BODIPY-CNOs**, deposited on mica. The height distribution analysis of about 100 individual CNOs is plotted in Figure 6c and clearly reveals the predominance of CNOs with an average diameter of 5 nm and a few larger CNOs.

TEM was used in order to characterize the carbon nanomaterials and confirmed the initial conversion of nanodiamonds to CNOs. The presence of agglomerates of **BODIPY-CNOs** with a size of few hundred nm was confirmed by bright field (BF) TEM investigations (Figure 7a). HR-TEM analysis shows that individual CNOs have an average diameter of 5-7 nm, with 6-8 concentric graphitic shells, 3.4 Å apart (Figure 7b, Figure S4). A few larger particles were found, up to 13 nm and 14 concentric graphitic shells. For all the samples EEL spectra at the carbon K-edge region (270-360 eV energy loss) show the typical near-edge fine structure for CNOs (Figure 7c, Figure S4), with a narrow peak corresponding to the $1s \rightarrow \pi^*$ transition (285 eV), indicating predominantly sp^2 -bonded carbons and a weaker peak at about 292 eV, corresponding to a $1s \rightarrow \sigma^*$ transition.⁵⁵

In vitro toxicity investigation and cellular biodistribution of CNOs in MCF-7 cells

In order to investigate the *in vitro* toxicity of different preparations of CNOs, the metabolic activity of MCF-7 cells was determined upon exposure to increasing concentrations of **benz-CNOs** and **BODIPY-CNOs** (from 0.5 to 10 $\mu\text{g/mL}$). Cell viability was measured after 24, 48, and 72 hours of incubation using the WST-8 test (Water-Soluble Tetrazolium salt) (Figure 8). The administration of functionalized CNOs did not affect the cellular viability as compared with the cell control (Figure 8a), even after prolonged exposure (72h) (Figure 8a and b).

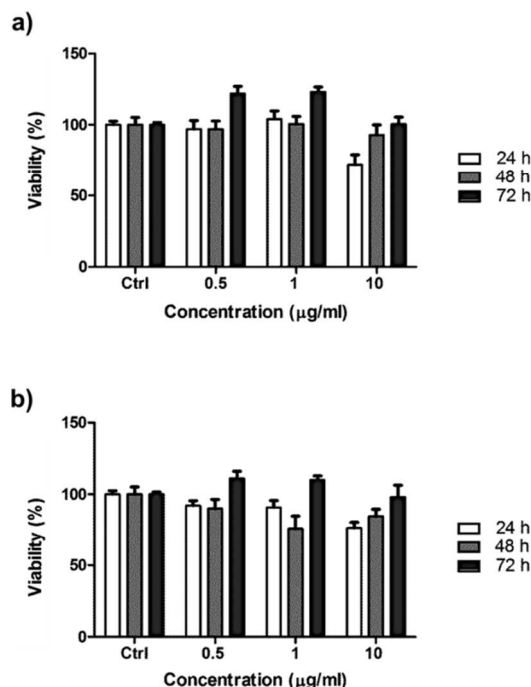


Fig. 8 Cellular viability of MCF-7 cells after exposure to different CNOs. Viability of MCF-7 cells exposed to CNOs was evaluated by the WST-8 assay. Viability of CNO treated cells was expressed relative to non-treated control cells (Ctrl). Viability of cells treated for 24, 48, and 72 hours (a) with 0.5, 1, and 10 $\mu\text{g/mL}$ **benz-CNOs** and (b) with 0.5, 1, and 10 $\mu\text{g/mL}$ **BODIPY-CNOs**.

To visualize the intracellular distribution of CNOs, confocal live cell imaging was performed using fluorescent **BODIPY-CNOs**. Representative images of the subcellular localization of **BODIPY-CNOs** (10 $\mu\text{g/mL}$) in living MCF-7 cells treated for 48 hours with the nanoparticles are shown in Figure 9. The CNOs were efficiently taken up by the cells and were found to localize predominantly in the cytoplasm and in the perinuclear region (Figure 9a, d). To probe the intracellular fate of CNOs in higher

detail, the distribution of **BODIPY-CNOs** into vesicular compartments was analyzed in living cells in combination with the LysoTracker probe, a specific marker of lysosomes (Figure 9b, e). As highlighted by the yellow colocalization signals in Figure 9c and f, **BODIPY-CNOs** localize in lysosomal vesicles, in line with previous reports on nanoparticles.^{56,57} Conversely, unconjugated **BODIPY 2** showed only weak staining of cellular membranes (data not shown), as **BODIPY** is an intrinsically lipophilic fluorescent dye.⁵⁸

The internalization of CNOs in the lysosomes was also confirmed by colocalization analysis. Figure S5 B shows the white colocalization mask applied to the image of Bodipy-CNOs and lysosomes in Figure S5 A. The white signal (Figure S5 B a and b) represents the overlapping regions of green CNOs and red lysosomal signals that are also represented in the middle area of the scatter plot (Figure S5 B c). Pearson's correlation coefficient (PCC) was used to quantify the degree of colocalization. The PCC measured was 0.7892.

In Figure S6 some representative stacks of the optical sectioning of a cell incubated with **BODIPY-CNOs** (10 $\mu\text{g}/\text{mL}$) and LysoTracker are shown. The signal of the internalized CNOs matches with the signal of the lysosomes throughout the entire volume of the cell. The movie of the complete z-stack acquired is shown in the supplementary Movie M1.

In summary, the presented data verify that CNOs can abundantly enter cells without exerting toxic effects on the investigated

MCF-7 cells (although further studies are needed to completely elucidate this point). The CNO nanomaterials are internalized by endocytosis and do not enter the nucleus of the cells.

30 Conclusions

Boron dipyrromethene (**BODIPY**) functionalized CNO conjugates have been synthesized and characterized. The high fluorescence of the nanoparticles allowed high-resolution imaging in MCF-7 human breast cancer cells. The CNOs were efficiently taken up by the cells and localized in lysosomes. Cell viability measured up to 72 hours following incubation did not show significant cytotoxicity. **BODIPY-CNO** conjugates have the necessary characteristics for further development of theranostic nano-platforms which combine targeting, imaging and therapeutic capabilities, due to their low cytotoxicity and the low fluorescence quenching of attached fluorescence probes. In combination with the synthetic versatility of **BODIPY** dyes, CNOs are very promising for the future preparation of various biological and theranostic applications.

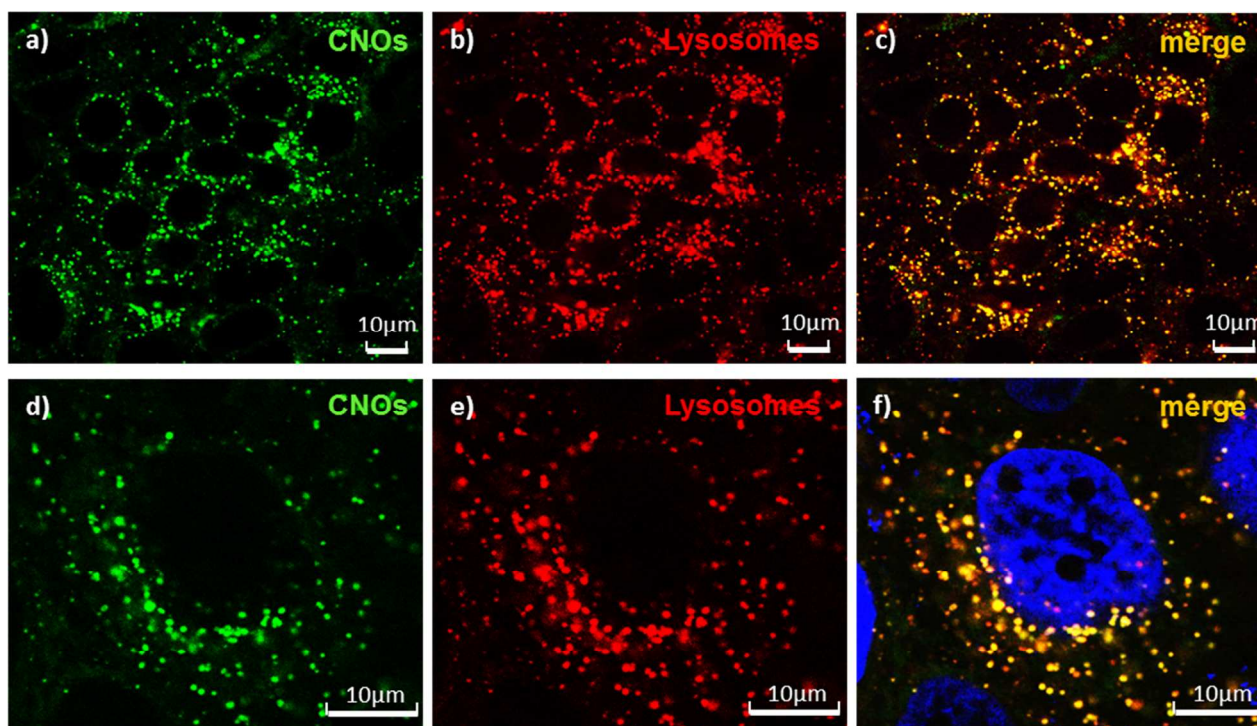


Fig. 9 Cellular uptake of **BODIPY-CNO** nanoparticles visualized by confocal microscope imaging in living cells. Representative confocal images of MCF-7 cells incubated for 48 hours with 10 $\mu\text{g}/\text{mL}$ **BODIPY-CNOs**. (a-c) Large field of view with several cells, and (d-f) imaging at single cell resolution. (a, d) green fluorescent **BODIPY-CNOs**, (b, e) lysosomes stained with LysoTracker Red probe, (c) merged images. Hoechst 33342 was used for vital staining of the nucleus (f). Note the high level of **BODIPY-CNO** uptake, and the colocalization (yellow) of the **BODIPY-CNO** within the lysosomes.

Experimental

Materials and Methods:

All starting materials, reagents and solvents were purchased from Sigma-Aldrich in high-purity grade and used without further purification. Spectrophotometric or HPLC grade solvents were used for UV-vis and fluorescence studies. All measurements were performed at room temperature and ambient conditions, unless otherwise noted. All instrumental details and additional procedures are summarized in the ESI.

Synthetic Procedures:

1: BODIPY fluorophore **1** was synthesized following a previously published procedure.⁴³

2: Benzoic acid (122.1 mg / 1.00 mmol), NHS (115.1 mg / 1.00 mmol), DCC (206.3 mg / 1.00 mmol) and DMAP (122.2 mg / 1.00 mmol) were dissolved in 40 mL of dry THF at 0°C under a N₂ atmosphere. The solution was allowed to warm up to room temperature and stirred for another 5 h. Then, **1** (67 mg / 0.20 mmol) dissolved in 10 mL of dry, deoxygenated THF was added and the reaction mixture was stirred at room temperature for 5 days. The solution was filtered and after evaporation of the THF, the crude was purified by column chromatography (SiO₂, hexane/dichloromethane (DCM) 3:1 (v/v) with rising amounts of DCM). **2** was obtained as a bright orange solid in 33% yield (29 mg / 0.065 mmol). X-ray quality crystals were obtained as orange rhombic plates by re-crystallizing from dichloromethane/methanol 1:3 (v/v) in the freezer (-20°C).

¹H NMR (400 MHz, CDCl₃) δ 8.23 (d, 2H, *J* = 8.3 Hz), 7.67 (t, 1H, *J* = 7.5 Hz), 7.54 (t, 2H, *J* = 7.8 Hz), 7.37 (m, 4H), 6.01 (s, 2H), 2.57 (s, 6H), 1.48 (s, 6H). ¹³C NMR (100 MHz, CDCl₃) (14.6, 121.4, 122.7, 126.6, 128.6, 128.7, 129.3, 130.2, 131.5, 132.6, 133.9, 140.1, 143.2, 151.6, 155.8). HRMS-ESI: *m/z*: calcd. for C₂₆H₂₄BF₂N₂O₂⁺: 445.1899 [M + H]⁺, found: 445.1911.

Benz-CNO: NaNO₂ (1.47 g / 21.3 mmol) was dissolved in 20 mL deionized (DI) water and cooled to 0°C. This solution was added at once to a solution of 4-aminobenzoic acid (2.88 g / 21.0 mmol) in 30 mL DMF at 0°C. 200 μL conc. HCl was added as the mixture was stirred for 30 min at 0°C. **p-CNOs**^{44,45,46} (31 mg) were dispersed in 20 mL DMF by ultrasonication for 20 min and the dispersion was added to the reaction mixture, which was stirred at 0°C for 4h and at RT for an additional 3 days. Following this, the CNOs were separated from the reaction mixture by centrifugation (30 min, 2100 g) and purified by subsequent re-dispersion – centrifugation steps in DI water, DMF, and methanol. After drying at 60°C overnight, 25 mg of **benz-CNOs** were recovered.

BODIPY-CNO: **Benz-CNOs** (10 mg) were dispersed in 20 mL dry THF and the dispersion was deoxygenated with N₂. Then NHS (9.2 mg / 0.08 mmol), DMAP (12.0 mg / 0.08 mmol) and EDC (12.4 mg / 14 μL / 0.08 mmol) were added and the mixture was heated under reflux for 1 h. Following this, **1** (13.6 mg / 0.04 mmol) was added and the reaction mixture was heated for another 44 h under reflux. After cooling to room temperature, the CNOs were precipitated by centrifugation (30 min / 2100 g) and separated from the supernatant. Subsequently, the solid was re-

dispersed by brief ultrasonication in THF and again centrifuged. This process was repeated for an additional four times. The obtained solid was dried at 60°C overnight. Approx. 12 mg of **BODIPY-CNOs** were recovered.

⁶⁰ CNO preparation for cellular studies:

Benz- and **BODIPY-CNOs** were dispersed in DMSO (1 mg/mL) and intensively sonicated as previously described.²³ For cellular *in vitro* experiments, all CNOs preparation were sonicated for 15 min at 50 kHz (100% intensity), diluted to the desired concentrations in a cell culture medium (DMEM), and sonicated 15 min at 50 kHz before adding to the cells.

Cell cultures:

MCF-7 cells (human mammary gland adenocarcinoma cell line ATCC HTB-22) were cultivated in DMEM with 50 μM glutamine, supplemented with 10% FBS, 100 U mL⁻¹ penicillin and 100 mg mL⁻¹ streptomycin. Cells were incubated in a humidified and controlled atmosphere with a 95% to 5% ratio of air/CO₂, at 37 °C.

WST-8 assay:

MCF-7 cells were seeded in 96 well microplates at a density of 5000 cells per well at a final volume of 100 μl and incubated for 24 h in a humidified atmosphere at 37 °C and 5% CO₂ to obtain a subconfluent monolayer (60–70% of confluence). The culture medium was removed and replaced with 100 μl of medium containing CNOs at the final concentrations of 0.5, 1, and 10 μg/mL. The metabolic activity of all cultures was determined after 24, 48 and 72 h of exposure to CNOs, using a standard WST-8 assay (Sigma). Assays were performed following the procedure previously described.⁵⁹ Data were expressed as mean ± SD. Differences in cell proliferation between cells treated with CNOs and the control were considered statistically significant with a *p*-value <0.05.

Confocal microscopy:

Fluorescence imaging was performed with a SP8-STED microscope (Leica Microsystems, GmbH, Germany) using a 63× oil immersion objective (HC PL APO CS2 63x/1.40 OIL). **BODIPY-CNOs** were excited at 488 nm and the emission was acquired in the spectral window 500-560 nm. Lysosomes were imaged by exciting the LysoTracker Red DND-99 with the 577 nm line of the white light laser (WLL, Leica), and acquired in the emission range of 600-680 nm. The nucleus stained with Hoechst 33342 (Sigma) was excited with the 405 nm wavelength and acquired at 415-480 nm.

CNOs incubation for cellular imaging:

MCF-7 cells were seeded in 3.5 cm glass bottom dishes (World Precision Instruments, FD35-100) and incubated for 24 h in a humidified atmosphere at 37 °C and 5% CO₂ to obtain a subconfluent monolayer (60–70% of confluence). After 24 h the medium was removed, and the cells were incubated with a suspension of **BODIPY-CNOs** (10 μg/mL). As a control, cells were left untreated (not shown). After 48 h of incubation at 37 °C with CNOs, the cells were washed three times with PBS (pH 7.4) and incubated for 30 minutes with 75 nM LysoTracker Red DND-99 (L7528, Life Technologies). The medium was then

replaced with fresh medium and the cells were transferred to the microscope incubator (Life Imaging Services, Switzerland). The temperature was maintained at 37 °C using the Cube and Box temperature control system, and the humidified 5% CO₂ atmosphere was maintained using an automated gas mixer system (The Brick; Life Imaging Services).

Acknowledgements

We are grateful to the Istituto Italiano di Tecnologia (IIT) for funding. The authors wish to thank Dr. Agustin Molina-Ontario (UTEF) for the preparation of the pristine CNOs; Dr. Marco Frascioni, Dr. Marco Salerno, Dr. Farouk Ayadi, Sine Mandrup Bertozzi, Giammarino Pugliese (IIT Genova) for instrumental support and helpful discussions. LE wishes to thank the NSF, PREM Program (DMR-1205302) and the Robert A Welch Foundation (Grant AH-0033) for generous support.

Notes and references

^a Istituto Italiano di Tecnologia (IIT), Nano Carbon Materials, Nanophysics Department, Via Morego 30, 16163 Genova, Italy. Tel: +39 – 010 – 71781 – 507; E-mail: silvia.giordani@iit.it

^b Istituto Italiano di Tecnologia (IIT), Center for Bio-Molecular Nanotechnology, Via Barsanti, 73010 Arnesano (Lecce), Italy.

^c Istituto Italiano di Tecnologia (IIT), Nanochemistry Department, Via Morego 30, 16163 Genova, Italy.

^d Istituto Italiano di Tecnologia (IIT), Center for Nano Science and Technology (CNST), Via G. Pascoli 70/3, 20133 Milano, Italy.

^e Department of Chemistry, Materials and Chemical Engineering “Giulio Natta”, Politecnico di Milano, Via Mancinelli 7, 20131 Milano, Italy.

^f Department of Chemistry, University of Texas at El Paso, 500 W. University Ave., El Paso, TX 79968, USA.

† Electronic Supplementary Information (ESI) available: Additional experimental and crystallographic data, additional confocal microscopy and HR-TEM images and illustrations, EELS, TGA, DLS and Z-potential results. Movie M1. See DOI: 10.1039/b000000x/

‡ Crystallographic data for **2**: CCDC: 1015701, C₂₆H₂₃N₂O₂F₂B, M = 444.27, orthorhombic F, *a* = 18.4695(18), *b* = 43.010(4), *c* = 10.9507(11) Å, α = β = γ = 90°, *V* = 8699.0(15) Å³, *T* = 100 K, space group *Fdd2*, *Z* = 16, 6167 reflections measured, 2757 independent (*R*_{int} = 0.043). The final *wR*(*F*₂) was 0.154.

- C. Fabbro, H. Ali-Boucetta, T. Da Ros, K. Kostarelos, A. Bianco and M. Prato, *Chem. Commun.*, 2012, **48**, 3911.
- B. S. Wong, S. L. Yoong, A. Jagusiak, T. Panczyk, H. K. Ho, W. H. Ang and G. Pastorin, *Adv. Drug. Deliv. Rev.*, 2013, **65**, 1964.
- N. Saito, H. Haniu, Y. Usui, K. Aoki, K. Hara, S. Takanashi, M. Shimizu, N. Narita, M. Okamoto, S. Kobayashi, H. Nomura, H. Kato, N. Nishimura, S. Taruta and M. Endo, *Chem. Rev.*, 2014, **114**, 6040.
- A. Montellano, T. Da Ros, A. Bianco and M. Prato, *Nanoscale*, 2011, **3**, 4035.
- J. Luczkowiak, A. Munoz, M. Sanchez-Navarro, R. Ribeiro-Viana, A. Ginieis, B. M. Illescas, N. Martin, R. Delgado and J. Rojo, *Biomacromolecules*, 2013, **14**, 431.
- J. Shi, X. Yu, L. Wang, Y. Liu, J. Gao, J. Zhang, R. Ma, R. Liu and Z. Zhang, *Biomaterials*, 2014, DOI: 10.1016/j.biomaterials.2013.08.049.
- Z. Liu, S. Tabakman, K. Welcher and H. Dai, *Nano Res.*, 2009, **2**, 85.
- K. Kostarelos, A. Bianco and M. Prato, *Nat. Nanotech.*, 2009, **4**, 627.
- V. N. Mochalin, O. Shenderova, D. Ho and Y. Gogotsi, *Nat. Nanotech.*, 2012, **7**, 11.
- Y. Zhu, J. Li, W. Li, Y. Zhang, X. Yang, N. Chen, Y. Sun, Y. Zhao, C. Fan and Q. Huang, *Theranostics*, 2012, **2**, 203.
- H. Zhang, G. Grüner and Y. Zhao, *J. Mater. Chem. B*, 2013, **1**, 2542.
- L. Feng, L. Wu and X. Qu, *Adv. Mater.*, 2013, **25**, 168.

- D. Ugarte, *Nature*, 1992, **359**, 707.
- J. Bartelmess and S. Giordani, *Beilstein J. Nanotechnol.*, 2014, accepted.
- A. Hirata, M. Igarashi and T. Kaito, *Tribol. Int.*, 2004, **37**, 899.
- L. Joly-Pottuz, N. Matsumoto, H. Kinoshita, B. Vacher, M. Belin, G. Montagnac, J. M. Martin and N. Ohmae, *Tribol. Int.*, 2008, **41**, 69.
- J. Luszczyn, M. E. Plonska-Brzezinska, A. Palkar, A. T. Dubis, A. Simionescu, D. T. Simionescu, B. Kalska-Szostko, K. Winkler and L. Echevoyen, *Chem. Eur. J.*, 2010, **16**, 4870.
- J. Brezcko, M. E. Plonska-Brzezinska and L. Echevoyen, *Electrochim. Acta*, 2012, **72**, 61.
- N. Keller, N. I. Maksimova, V. V. Roddatis, M. Schur, G. Mestl, Y. V. Butenko, V. L. Kuznetsov and R. Schlögl, *Angew. Chem. Int. Ed.*, 2002, **41**, 1885.
- D. Pech, M. Brunet, H. Durou, P. Huang, V. Mochalin, Y. Gogotsi, P.-L. Taberna and P. Simon, *Nature Nanotech.*, 2010, **5**, 651.
- Y. Gao, Y. S. Zhou, M. Qian, X. N. He, J. Redepenning, P. Goodman, H. M. Li, L. Jiang and Y. F. Lu, *Carbon*, 2013, **51**, 52.
- M. E. Plonska-Brzezinska, D. M. Brus, A. Molina-Ontaria and L. Echevoyen, *RSC Adv.*, 2013, **3**, 25891.
- M. Yang, K. Flavin, I. Kopf, G. Radics, C. H. A. Hearnden, G. J. McManus, B. Moran, A. Villalta-Cerdas, L. A. Echevoyen, S. Giordani and E. C. Lavelle, *Small*, 2013, **9**, 4194.
- P. Singh, S. Campidelli, S. Giordani, D. Bonifazi, A. Bianco and M. Prato, *Chem. Soc. Rev.*, 2009, **38**, 2214.
- K. Flavin, M. N. Chaur, L. Echevoyen and S. Giordani, *Org. Lett.*, 2010, **12**, 840.
- J. L. Bahr, J. Yang, D. V. Kosynkin, M. J. Bronikowski, R. E. Smalley and J. M. Tour, *J. Am. Chem. Soc.*, 2001, **123**, 6536.
- A. Loudet and K. Burgess, *Chem. Rev.*, 2007, **107**, 4891.
- G. Ulrich, R. Ziessel and A. Harriman, *Angew. Chem. Int. Ed.*, 2008, **47**, 1184.
- Q. Zheng, G. Xu and P. N. Prasad, *Chem. Eur. J.*, 2008, **14**, 5812.
- K. E. Beatty, J. Szychowski, J. D. Fisk and D. A. Tirell, *ChemBioChem*, 2011, **12**, 2137.
- A. Romieu, C. Massif, S. Rihn, G. Ulrich, R. Ziessel and P.-Y. Renard, *New. J. Chem.*, 2013, **37**, 1016.
- C. Y. Lee and J. T. Hupp, *Langmuir* 2010, **26**, 3760.
- O. A. Bozdemir, S. Erbas-Cakmak, O. O. Ekiz, A. Dana and E. U. Akkaya, *Angew. Chem. Int. Ed.*, 2011, **50**, 10907.
- J. Iehl, J.-F. Nierengarten, A. Harriman, T. Bura and R. Ziessel, *J. Am. Chem. Soc.*, 2012, **134**, 988.
- M. E. El-Khouly, S. Fukuzumi and F. D'Souza, *ChemPhysChem*, 2014, **15**, 30.
- J. Bartelmess, A. J. Francis, K. A. El Roz, F. N. Castellano, W. W. Weare and R. D. Sommer, *Inorg. Chem.*, 2014, **53**, 4527.
- S. G. Awuah and Y. You, *RSC Adv.*, 2012, **2**, 11169.
- A. Kamkaev, S. H. Lim, H. B. Lee, L. V. Kiew, L. Y. Chung and K. Burgess, *Chem. Soc. Rev.*, 2013, **42**, 77.
- A. B. Nepomnyashchii and A. J. Bard, *Acc. Chem. Res.*, 2012, **45**, 1844.
- N. Boens, V. Leen and W. Dehaen, *Chem. Soc. Rev.*, 2012, **41**, 1130.
- K. Krumova and G. Cosa, *J. Am. Chem. Soc.*, 2010, **132**, 17560.
- J. Bartelmess, W. W. Weare, N. Latortue, C. Duong and D. S. Jones, *New. J. Chem.*, 2013, **37**, 2663.
- J. Bartelmess and W. W. Weare, *Dyes Pigm.*, 2013, **97**, 1-8.
- V. L. Kuznetsov, M. N. Aleksandrov, I. V. Zagoruiko, A. L. Chuvilin, E. M. Moroz and V. N. Kolomiichuk, *Carbon*, 1991, **29**, 665.
- V. L. Kuznetsov, A. L. Chuvilin, Y. V. Butenko, I. Y. Mal'kov and V. M. Titov, *Chem. Phys. Lett.*, 1994, **222**, 343.
- A. Palkar, F. Melin, C. M. Cardona, B. Elliott, A. K. Naskar, D. D. Edie, A. Kumbhar and L. Echevoyen, *Chem. Asian J.*, 2007, **2**, 625.
- J. Bartelmess, B. Ballesteros, G. de la Torre, D. Kiessling, S. Campidelli, M. Prato, T. Torres and D. M. Guldi, *J. Am. Chem. Soc.*, 2010, **132**, 16202.
- K. Flavin, K. Lawrence, J. Bartelmess, M. Tasiar, C. Navio, C. Bittencourt, D. F. O'Shea, D. M. Guldi and S. Giordani, *ACS Nano*, 2011, **2**, 1198.
- T. Lazarides, S. Kuhri, G. Charalambidis, M. K. Panda, D. M. Guldi and A. G. Coutselos, *Inorg. Chem.*, 2012, **51**, 4193.

-
- 50 C. T. Cioffi, A. Palkar, F. Melin, A. Kumbhar, L. Echegoyen, M. Melle-Franco, F. Zerbetto, G. M. A. Rahman, C. Ehli, V. Sgobba, D. M. Guldi and M. Prato, *Chem. Eur. J.*, 2009, **15**, 4419.
- 51 V. V. Didenko, V. C. Moore, D. S. Baskin and R. E. Smalley, *Nano Lett.*, 2005, **5**, 1563.
- 52 B. Tian, C. Wang, S. Zhang, L. Feng and Z. Liu, *ACS Nano*, 2011, **5**, 7000.
- 53 Y. Liu, C.-y. Liu and Y. Liu, *Appl. Surf. Sci.*, 2011, **257**, 5513.
- 54 S. Giordani, J. Bartelmess, M. Frascioni, I. Biondi, S. Cheung, M. Grossi, D. Wu, L. Echegoyen and D. F. O'Shea, *J. Mater. Chem. B*, 2014, DOI:10.1039/C4TB01087F.
- 55 P. Redlich, F. Banhart, Y. Lyutovich and P. M. Ajayan, *Carbon*, 1998, **36**, 561.
- 56 S. Sabella, R. P. Carney, V. Brunetti, M. A. Malvindi, N. Al-Juffali, G. Vecchio, S. M. Janes, O. M. Bakr, R. Cingolani, F. Stellacci and P. P. Pompa, *Nanoscale*, 2014, **6**, 7052.
- 57 G. Leménager, E. De Luca, Y.-P. Sun and P. P. Pompa, *Nanoscale*, 2014, **6**, 8617.
- 58 *The Molecular Probes® Handbook—A Guide to Fluorescent Probes and Labeling Technologies*, ed. I. Johnson and M. T. Z. Spence, Life Technologies Corporation, Carlsbad (CA), 10th edn., 2010.
- 59 M. A. Malvindi, V. Brunetti, G. Vecchio, A. Galeone, R. Cingolani and P. P. Pompa, *Nanoscale*, 2012, **4**, 486.